

# The Repulsive Effect of Covariant Effective Quantum Gravity

Yan Liu<sup>†1</sup>, Jie Jiang<sup>‡2</sup>, Bing Sun<sup>\*3</sup>

<sup>†</sup> *Department of Physics, Yantai University, Yantai 264005, China*

<sup>‡</sup> *School of Physics and Astronomy, Beijing Normal University, Beijing 100875, China*

<sup>\*</sup> *Department of Basic Courses, Beijing University of Agriculture, Beijing 102206, China*

## Abstract

In this work we discuss the geodesic motion of covariant effective quantum black hole, and give the explicit critical values of the quantum parameter, beyond which the geodesic orbits disappear. By the analysis of the critical orbital behavior, we find that in covariant effective loop quantum gravity, there exists static free test particle levitating outside the black hole, and, different with the attractive effect performed by the classical gravity, the quantum correction in the general relativity could perform as the repulsive effect in certain regions.

---

<sup>1</sup>email: yanliu@ytu.edu.cn

<sup>2</sup>email: jiejiang@mail.bnu.edu.cn

<sup>3</sup>email: bingsun@bua.edu.cn, corresponding author

# Contents

<b>1</b>	<b>Introduction</b>	<b>1</b>
<b>2</b>	<b>Review of the two black hole models in covariant EQG</b>	<b>2</b>
<b>3</b>	<b>Circular orbits</b>	<b>3</b>
3.1	Generic circular motion . . . . .	3
3.2	Marginal circular orbit . . . . .	6
<b>4</b>	<b>Motion with turning points</b>	<b>7</b>
<b>5</b>	<b>Conclusion and discussion</b>	<b>12</b>

## 1 Introduction

In recent years, direct experimental evidence for the predictions of Einstein’s General Relativity (GR) has grown significantly. Astrophysical observations, such as the lunar laser ranging [1] and evolution of planetary orbits [2], have confirmed the validity of GR in the weak field regime. Meanwhile, the detection of gravitational waves from binary black hole mergers [3] and the first image of a black hole shadow by the Event Horizon Telescope [4] stand as compelling confirmations of GR’s accuracy in the strong field regime. Despite these successes, longstanding theoretical challenges remain, such as the singularity problem and the difficulty of reconciling GR with quantum field theory. These unresolved issues have motivated substantial efforts to develop quantum modifications of gravity [5–8].

Canonical quantum gravity as a candidate of quantum gravity, provides a complete treatise of the canonical quantization of GR [9], such as those underlying loop quantum gravity, advances the idea of a non-perturbative, background-independent quantization of spacetime in effective Hamiltonian theory [10, 11]. However, it has been challenging to maintain diffeomorphism covariance in these effective Hamiltonian frameworks [12]. Recently, Zhang et al. [13] made significant progress in this direction. They presented a covariant effective quantum gravity (EQG) formulation that maintains diffeomorphism covariance while introducing a controllable quantum parameter into the gravitational dynamics. Their analysis led to two quantum-corrected spherically symmetric black hole solutions, providing an ideal arena to investigate how quantum effects might alter gravitational properties in a covariant setting.

A natural starting point for probing the implications of the quantum parameter on spacetime is to examine the geodesic motion of test particles. Studies on geodesic motion are instrumental in understanding astrophysical processes, such as binary inspirals and gravitational wave signals [14–16], the shadow of black holes [17, 18], Penrose process [19], accretion disk [20], and the distribution of dark matter [21] around compact objects. In GR and some of its modifications,

gravity remains strictly attractive for ordinary matter sources, and the conclusion often reinforced by analyzing particle trajectories near black holes [22–28]. Nevertheless, under extreme conditions particularly at small scales where quantum effects are expected to dominate, this classical picture may no longer hold [29].

In this work, we investigate the geodesic motion of massive test particles in the covariant EQG black hole spacetimes introduced in [13]. Our analysis strictly reveals an suppressing phenomenon: beyond a critical value of the quantum parameter, the gravitational field can exhibit effectively repulsive behavior. This stark departure from classical expectations emphasizes the importance of carefully incorporating quantum corrections while preserving covariance. By demonstrating that even well motivated, diffeomorphism covariant quantum modifications can produce repulsive gravitational effects, we raise new questions about the fundamental nature of gravity at the Planckian frontier and beyond.

## 2 Review of the two black hole models in covariant EQG

The two static black hole solutions in [13] are given by

$$ds_1^2 = -f_1(r)dt^2 + \frac{dr^2}{f_1(r)} + r^2 d\theta^2 + r^2 \sin^2 \theta d\phi^2, \quad (2.1)$$

$$ds_2^2 = -f_2(r)dt^2 + \frac{dr^2}{\mu_2(r)f_2(r)} + r^2 d\theta^2 + r^2 \sin^2 \theta d\phi^2, \quad (2.2)$$

with

$$f_1(r) = 1 - \frac{2M}{r} + \frac{\alpha^2}{r^2} \left(1 - \frac{2M}{r}\right)^2, \quad (2.3)$$

$$f_2(r) = 1 - \frac{2M}{r}, \quad \mu_2(r) = 1 + \frac{\alpha^2}{r^2} f_2(r), \quad (2.4)$$

where  $M$  is the mass of the covariant black holes, and  $\alpha$  is the quantum parameter. The outer event horizons  $r_{1+} = r_{2+} = 2M$  are independent of the quantum parameter. While the inner horizons are given by

$$r_{1-} = r_{2-} = \frac{A}{3} - \frac{\alpha^2}{A}, \quad (2.5)$$

$$A^3 = 3\alpha^2(9M + \sqrt{81M^2 + 3\alpha^2}). \quad (2.6)$$

As the parameter  $\alpha$  increases to infinity, the inner horizon asymptotically close to the outer horizon, which indicates that when the mass of the black hole  $M$  is small as in the quantum scale level, the black hole is nearly extreme. When  $\alpha = 0$ , the inner horizon vanishes, and turns out to be the physical singularity at  $r = 0$ .

Since the spacetime is spherically symmetric, we consider the motion on the equatorial plane, such that  $\theta = \pi/2$  and  $\dot{\theta} = 0$ . On the equatorial plane, the behavior of geodesics are dominated by the radial motion  $\dot{r} = \pm\sqrt{R(r)}$ , where the  $+$  and  $-$  sign denotes the ingoing and outgoing trajectories, and the radial potential  $R(r)$  in the two black hole spacetime models are given by

$$R_1(r) = E^2 - f_1(r)\left(1 + \frac{L^2}{r^2}\right), \quad (2.7)$$

$$R_2(r) = \mu_2(r)E^2 - f_2(r)\mu_2(r)\left(1 + \frac{l^2}{r^2}\right), \quad (2.8)$$

where  $E$  and  $L$  are the conserved energy and orbital angular momentum of the particle per unit mass. It is interesting that the roots of  $R_2(r)$  is independent of  $\alpha$ . We can rewrite  $R_2(r)$  as

$$R_2(r) = \frac{\mu_2(r)}{r^3}V_{eff}, \quad (2.9)$$

$$V_{eff} = L_2^2(2M - r) + r^2(2M + (-1 + E_2^2)r), \quad (2.10)$$

in which the key term deciding the roots is actually  $V_{eff}$  outside of the horizon, which is exactly the effective potential of the radial motion in Schwarzschild spacetime, as the case of  $\alpha = 0$  for  $ds_1$  spacetime, such that the behavior of  $R_2(r)$  is as same as  $R_1(r, \alpha = 0)$ , so do  $\frac{dR_2(r)}{dr}$  and  $\frac{d^2R_2(r)}{dr^2}$ . Therefore, in the following sections we mainly focus on the first model of the  $ds_1$  spacetime. For simplicity, in the following sections we set  $M = 1$  in the plots.

## 3 Circular orbits

### 3.1 Generic circular motion

For generic circular geodesic motion, the radial potential satisfies

$$R_1(r) = 0, \quad \frac{dR_1(r)}{dr} = 0. \quad (3.1)$$

By solving the equations Eq.(3.1) above, we obtain the conserved energy and angular momentum of the circular motion given by

$$E_1(r_*, \alpha) = \frac{\sqrt{(L_1^2 + r_*^2)(r_* - 2M)(r_*^3 + \alpha^2(r_* - 2M))}}{r_*^3} \quad (3.2)$$

$$L_1(r_*, \alpha) = \sqrt{\frac{r_*^2(r_*^3 M - (r_* - 2M)(r_* - 4M)\alpha^2)}{(r_* - 3M)(r_*^3 + 2\alpha^2(r_* - 2M))}}, \quad (3.3)$$

where  $r_*$  denotes the position of the circular motion. As well known in Schwarzschild spacetime, the innermost stable circular motion (ISCO) locates at  $r_{ISCO} = 6M$ , the unstable circular motion is allowed between the innermost circular orbit (ICO)  $r_{ICO} = 3M$  and  $r_{ISCO} = 6M$ , the stable circular motion exists beyond the ISCO. However, things are interestingly different in this case. Based on the analysis of the positive property of the formula inside the square root of  $L_1$ , we find that the position of the ISCO are still locates at  $r_{ICO} = 3M$ , due to the term  $r_* - 3M$  in the denominator of  $L_1$ , which are independent of the quantum correction  $\alpha$ . However, the circular motion are not always permitted beyond ICO due to the quantum parameter  $\alpha$ .

The positive property of  $L_1^2$  is decided by the cubic polynomial

$$\beta = r_*^3 M - (r_* - 2M)(r_* - 4M)\alpha^2, \quad (3.4)$$

which implicates that there exists a critical value of the parameter  $\alpha = \alpha_c$ , beyond which the angular momentum of the circular motion is unreal.

By simply analyzing the structure of the polynomial  $\beta$ , we can roughly discuss the disappearance of the circular geodesic motion. In the region  $2M < r_* < 4M$ , the angular momentum of the circular motion is always real. In the region  $r_* > 4M$ , the angular momentum of the circular motion is real with the parameter  $\alpha < \alpha_c$ . However, when  $\alpha > \alpha_c$  in the region  $r_* > 4M$ , the angular momentum of the circular motion could be unreal, which implicates that the circular motion is not always allowed in this region, such that there exists some region, although beyond the ICO, in which no circular orbits exist, even the ISCO may not be allowed neither.

The explicit range of the "no circular" region can be obtained by finding the root of the cubic polynomial  $\beta$ (3.4). The discriminate of  $\beta$  is given by

$$\Delta_3 = \frac{4\alpha^4(\alpha^4 - 432M^4)}{M^2}. \quad (3.5)$$

When  $\alpha < 2 \times 3^{3/4}M$ , we have  $\Delta_3 < 0$ , there exists only one real root for  $\beta$  given by

$$r_{*1} = \frac{\alpha^2}{3M} - \frac{1}{3} \left( -\frac{\alpha^6}{M^3} + 3\sqrt{1296\alpha^4 M^2 - \frac{3\alpha^8}{M^2} + \frac{27\alpha^4}{M} - 108\alpha^2 M} \right)^{1/3} \quad (3.6)$$

$$- \frac{1}{3} \left( -\frac{\alpha^6}{M^3} - 3\sqrt{1296\alpha^4 M^2 - \frac{3\alpha^8}{M^2} + \frac{27\alpha^4}{M} - 108\alpha^2 M} \right)^{1/3} \leq r_+ \quad (3.7)$$

which implicates that outside of the horizon, we always have  $\beta \geq 0$ , such that the circular motion is always allowed.

When  $\alpha = 2 \times 3^{3/4}M$ , we have  $\Delta_3 = 0$ , the roots of  $\beta$  are given by

$$r_{*0} = r_{*2} = 2(\sqrt{3} + 3)M \approx 9.464M, \quad (3.8)$$

$$r_{*1} = 4(2\sqrt{3} - 3)M \approx 1.856M, \quad (3.9)$$

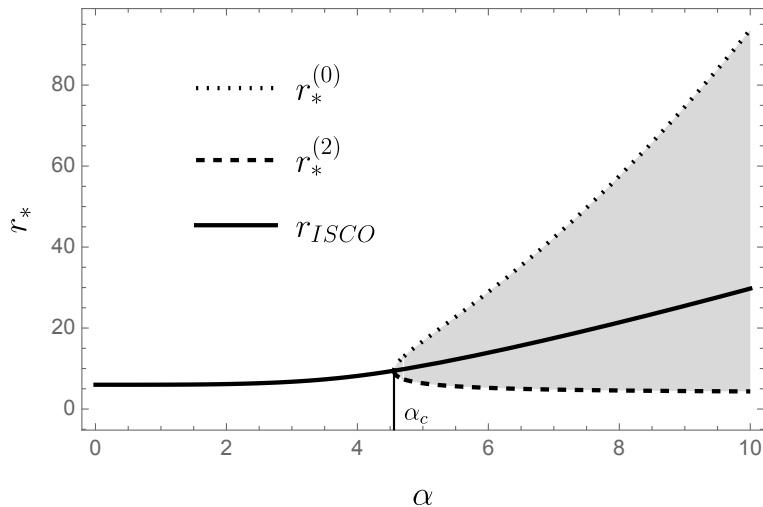


Figure 1: The disallowed region for circular motion.

which implicate that we always have  $\beta \geq 0$  outside of the horizon, therefore, the circular motion is always allowed.

When  $\alpha > 2 \times 3^{3/4}M$ , we have  $\Delta_3 > 0$ , there exists three distinct real roots for  $\beta$  given by

$$r_*^{(i)} = \frac{1}{3} \left( \alpha^2 - 2\alpha\sqrt{\alpha^2 - 18M^2} \cos\left(\frac{1}{3} \arccos\left(\frac{108M^4 - 27M^2\alpha^2 + \alpha^4}{\alpha\sqrt{(\alpha^2 - 18M^2)^3}}\right) + \frac{2\pi i}{3}\right) \right), \quad i = 0, 1, 2. \quad (3.10)$$

Note that  $r_*^{(0)} > r_*^{(2)} > r_+ > r_*^{(1)}$ , and when  $\alpha = 2 \times 3^{3/4}M$ , the roots  $r_*^{(0)}$  and  $r_*^{(2)}$  merge into a double root and expressed as that given in Eq.(3.8). In the range  $r_*^{(2)} < r_* < r_*^{(0)}$ , the polynomial  $\beta < 0$ , the angular momentum of the circular motion is unreal, which implicates that the circular motion is disallowed. In the range  $r_* > r_*^{(0)}$  and  $r_+ < r_* < r_*^{(2)}$ , the polynomial  $\beta > 0$ , such that the circular motion is allowed.

We conclude that the critical value of the parameter and the radius of critical circular motion are given by

$$\alpha_c = 2 \times 3^{3/4}M, \quad r_c = 2(\sqrt{3} + 3)M, \quad (3.11)$$

when  $\alpha > \alpha_c$ , the forbidden region for circular motion appears. As the parameter  $\alpha$  increases, the ISCO disappears at  $r_c$ , and then the stable and unstable circular motion are disallowed.

The position and conserved energy and angular momentum of the ISCO motion can be obtained by solving  $\frac{d^2R(r)}{dr^2} = 0$  combined with the solutions (3.2) and (3.3). In Figure 1, we show the disappearance of the circular motion, including the vanishing ISCO. The dotted line and the dashed line denote the boundary of the "no circular" region  $r_*^{(0)}$  and  $r_*^{(2)}$  respectively, between which in the gray region, the circular motion are not allowed. The black line denoting

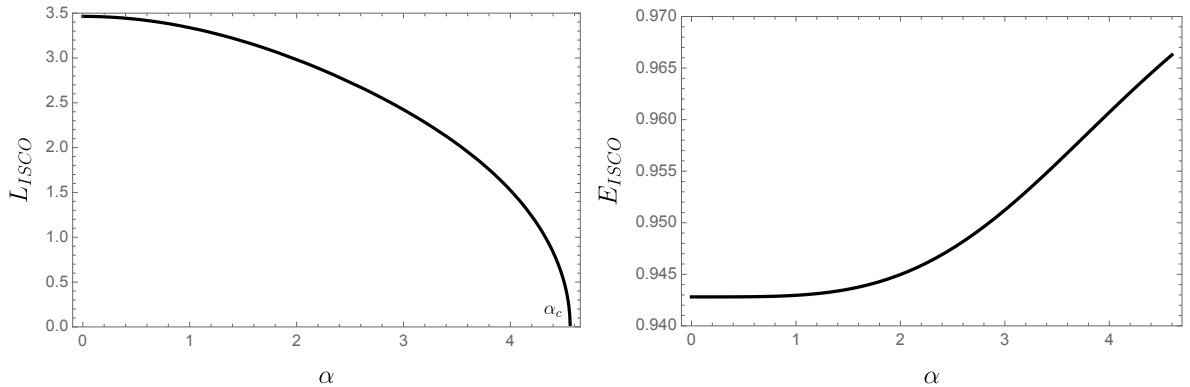


Figure 2: The variation of the angular momentum (left) and energy (right) of ISCO.

the position of ISCO,  $r_{ISCO}$ , intersecting with  $r_*^{(0)}$  and  $r_*^{(2)}$  at  $\alpha = \alpha_c$ . Note that in the region  $r_*^{(2)} < r < r_{ISCO}$  are the disallowed unstable circular orbits, and in the region  $r_{ISCO} < r < r_*^{(0)}$  are the disallowed stable circular orbits. Figure 1 shows clearly that ISCO moves far away from the original position due to the quantum correction. When  $\alpha > \alpha_c$ , the ISCO disappears first, then the stable and unstable circular motion disappear as the parameter  $\alpha$  increases. Note that when  $\alpha \rightarrow \infty$ , we have  $r_*^{(2)} \rightarrow 4M$ , which corresponds to our rough analysis before.

In Figure 2, we plot the variation of conserved energy and angular momentum of ISCO due to the increasing quantum correction  $\alpha$  in  $ds_1$  spacetime, from which we can see that when the parameter  $\alpha$  increases, while the energy of the ISCO monotonically increases, the angular momentum of ISCO monotonically decreases to zero and ends at  $\alpha = \alpha_c$ . This implicate that at this point, although the radial potential still satisfies zero conditions, including its first and second derivative, but the ISCO is not a circular motion, and turns out to be a rest particle hanging at  $r_c$ , since its angular momentum is zero. Similarly for those with  $\alpha > \alpha_c$ , the critical circular orbits turn to be a rest particle hanging at  $r_*^{(0)}$  or  $r_*^{(2)}$ .

When  $\alpha$  is small, the position, conserved energy, and angular momentum of the ISCO due to quantum correction are given by

$$r_{ISCO} = 6M + \frac{\alpha^4}{81M^3} + O(\alpha^6), \quad (3.12)$$

$$L_{ISCO} = 2\sqrt{3}M - \frac{2\alpha^2}{9\sqrt{3}M} + O(\alpha^4), \quad (3.13)$$

$$E_{ISCO} = \frac{2\sqrt{2}}{3} + \frac{\alpha^4}{4374\sqrt{2}M^4} + O(\alpha^6). \quad (3.14)$$

### 3.2 Marginal circular orbit

The marginal circular orbit (MCO) is the circular orbit with the energy  $E = 1$ , by solving (3.1), we show that the angular momentum and the location of the MCO motion  $L_m$  and  $r_m$

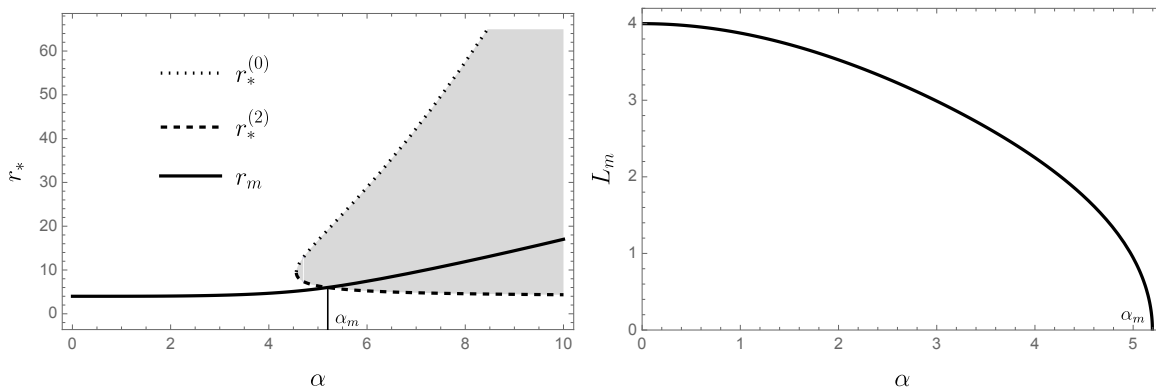


Figure 3: The disappearance (left) and the angular momentum (right) of MCO.

should satisfy

$$L_m = \sqrt{\frac{r^2(M(r^3 + 6r\alpha^2) - 8M^2\alpha^2 - r^2\alpha^2)}{(r - 3M)(r^3 - 4M\alpha^2 + 2r\alpha^2)}}, \quad (3.15)$$

$$r^4(-3M + r)(r^3 - 4M\alpha^2 + 2r\alpha^2) - (-2M + r)^2(r^3 - 2M\alpha^2 + r\alpha^2)^2 = 0. \quad (3.16)$$

Note that even though the expression of the  $L_m$  in Eq.(3.15) has same form with the generic circular case in Eq. (3.3), but MCO does not disappear at  $\alpha_c$ . In Figure 3 we show the disappearance and angular momentum of MCO motion due to the loop quantum correction  $\alpha$ . The line denoting MCO enter the gray region after intersecting with  $r_*^{(2)}$  at  $\alpha = \alpha_m$ . The explicit critical value for MCO can be obtained by solving  $r_m = r_*^{(2)}$  and given by

$$\alpha_m = 3\sqrt{3}M, \quad r_{mc} = 6M. \quad (3.17)$$

When  $\alpha > \alpha_m$ , MCO does not exist. Similarly with ISCO, the angular momentum of MCO monotonically decrease to zero with increasing  $\alpha$ , and ends at  $\alpha = \alpha_m$ .

When  $\alpha$  is small, the position and angular momentum of the MCO due to the quantum correction are given by

$$r_m = 4M + \frac{\alpha^4}{256M^3} + O(\alpha^6), \quad (3.18)$$

$$L_m = 4M - \frac{\alpha^2}{8M} + O(\alpha^4). \quad (3.19)$$

## 4 Motion with turning points

In the previous section, we show the disappearance of the circular motion. Based on the continuity of the motion in  $(E, L)$  phase space, the circular motion is a double root of the



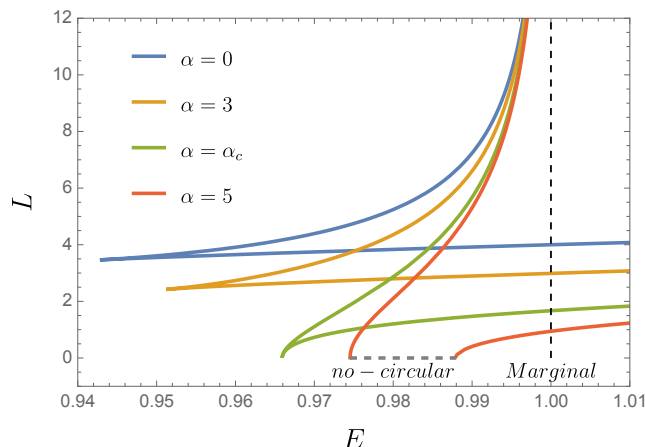


Figure 4: The  $(E, L)$  phase space of geodesic motion in  $ds_1$ .

radial potential, and could split into two single roots describing the turning points to form the root structure with trapped orbits, bound orbits and deflecting orbits as described in [23]. Therefore, it is naturally to deduce that there exists a region such that the generic trapped, plunging, bound and deflecting orbits disappear. For the convenience of discussion, we here in Table 1 introduce the root structure notation of the radial potential used in [23].

Notation	Denotes	Notation	Denotes
	outer horizon	•	simple roots (turning points)
+	allowed region	••	double roots (circular orbits)
-	disallowed region	•••	triple roots (ISCO)
>	radial infinity	•	roots touching the horizon

Table 1: Notations for the root structures of the radial potential.

In Figure 4, we show the  $(E, L)$  phase space of the geodesic motion. The colored curves are obtained based on the angular momentum and energy of the circular motion described by (3.2) and (3.3), plotted with  $r_*$  as the parameter. Each colored curve can be divided into two parts by ISCO at the vertex point, where the lower part describes the unstable circular orbits which energy can be extended to infinity as  $r_* \rightarrow r_{ICO}$ , and the upper part describes the stable circular orbits which angular momentum asymptotically to infinity and energy to 1 as  $r_* \rightarrow \infty$ .

Figure 4 describes the variation of the phase space due the parameter  $\alpha$ . When  $\alpha = \alpha_c$ , ISCO starts to disappear, and when  $\alpha > \alpha_c$ , the region that disallows the circular motion appears, eliminating parts of the stable and unstable circular motion, described by the thick gray dashed line in Figure 4. The root structures of the stable and unstable circular motion with  $E < 1$ ,  $|+\bullet-\bullet\bullet-|$  and  $|+\bullet\bullet+\bullet-|$ , contains not only circular motion with  $\bullet\bullet$ , but also the motion in the + region, such as trapped orbits in  $|+\bullet-\dots$ , the whirling trapped orbits

in  $| + \bullet$  and the homoclinic orbits in  $\bullet\bullet + \bullet$ , all of which share the same energy and angular momentum with the circular motion in the phase space. Therefore, the region that the circular orbits disappear, these kinds of orbits related to circular motion disappear as well.

The vertical black dashed line in Figure 4 denotes the marginal motion with energy  $E = 1$ , of which the cross points with the colored curves are marginal circular orbits. Note that when  $\alpha > \alpha_m$ , the "no-circular" region is beyond  $E = 1$ , and intersects with the Marginal dashed line, such that MCO and the unstable circular orbits with  $E > 1$  disappear, which are described by the root structure  $| + \bullet\bullet + \rangle$ . As we analyzed in the last paragraph, the corresponding whirling trapped orbits and whirling deflecting orbits  $\bullet\bullet + \rangle$  are forbidden as well.

The periodic bound motion are confined by circular and marginal motion in the triangle like region with root structure  $| + \bullet - \bullet + \bullet - \rangle$ . The turning points of bound orbits in structure  $\bullet + \bullet$  can be seen as the separation of the double root  $- \bullet\bullet -$  from the stable circular motion, or  $\bullet\bullet + \bullet$  from the unstable circular motion. By continuity in the phase space, when the circular motion disappear, in the neighborhood region of which, the bound motion disappear as well. As the red curve with  $\alpha > \alpha_c$  shown in Figure 4, one can imagine there exists a missing triangle-like horn region cut by the "no-circular" dashed line, the boundary of which are the disappeared circular motion, and inside the region of which, are the disappeared bound orbits. Similarly, when  $\alpha > \alpha_{mc}$ , due to the disappearance of the unstable circular motion  $| + \bullet\bullet + \rangle$ , the deflecting orbits in the second  $+$  region of  $| + \bullet - \bullet + \rangle$  disappear as well. In the following part, we investigate the non-existence of bound orbits as an example, and then extends to deflecting cases.

The turning points of the bounded motion are the pericenter  $r_p$  and apocenter  $r_a$ , satisfying

$$R_1(r_a) = R_1(r_p) = 0, \quad (4.1)$$

replacing  $r_a$  and  $r_p$  by the taxonomy of eccentricity  $e$  and semi-latus rectum  $p$  as

$$r_a = \frac{p}{1 - e}, \quad r_p = \frac{p}{1 + e}, \quad (4.2)$$

and solve (4.1), the energy and angular momentum of the bound motion are obtained given by

$$E = \frac{1}{p^3} \sqrt{(2(1+e)M - p)((1+e)^2L^2 + p^2)((2(1+e)M - p)(1+e)^2\alpha^2 - p^3)}, \quad (4.3)$$

$$L = \sqrt{\frac{p^2(Mp^3 - (4M - p)(2(1+e^2)M - p)\alpha^2)}{(p - ((3 + e^2)M))(p^3 + 2(p + e^2p - 2M - 6e^2M)\alpha^2)}}. \quad (4.4)$$

The angular momentum of bound orbits are real when  $\alpha < \alpha_{bc}$ , where the critical parameter  $\alpha_{bc}$  for the bound motion is given by

$$\alpha_{bc} = \sqrt{\frac{Mp^3}{(4M - p)(2M(1 + e^2) - p)}}. \quad (4.5)$$

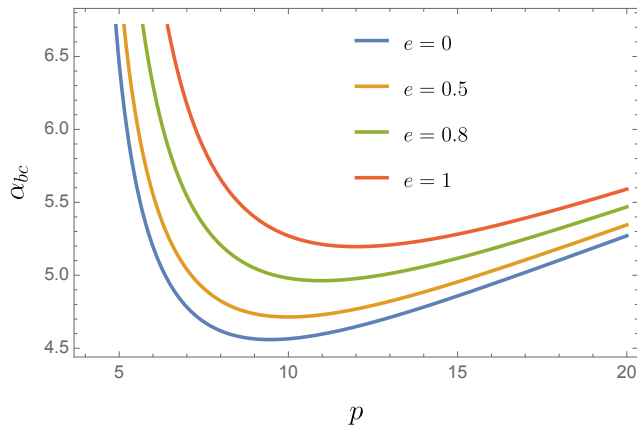


Figure 5: The critical value  $\alpha_{bc}$  in terms of  $e$  and  $p$  for bound orbital motion.

In Figure 5, we show the critical value  $\alpha_{bc}$  as a function of  $e$  and  $p$ . In the case  $e = 0$ , the two turning points merge into a double root as  $-\bullet\bullet-$ , such that  $r_a = r_p = r_* = p$  and here  $p$  denoting the radius of the stable circular motion, and note that the minimum value of the curve is exactly  $\alpha_c$ . As the eccentricity increases in  $0 < e < 1$ , such as the cases  $e = 0.5$  and  $e = 0.8$ , the critical value of the parameter  $\alpha_{bc}$  increases, denoting the start point of the vanishing bound orbits. Note that for the cases with  $0 < e < 1$ , the minimum value of each curve is exactly the critical points denoting the disappearance of unstable circular motion and the corresponded homoclinic orbits in  $\bullet\bullet+\bullet$ , where the pericenter  $r_p$  merge with the first turning point of the trapped orbits to be a double root denoting the unstable circular orbit, and the  $+$  region between the apocenter and the double root are the homoclinic orbits. The case  $e = 1$  describes the disappearance of the marginal motion with energy  $E = 1$ , the minimum value of which is exactly the critical parameter  $\alpha_m$  for MCO, where the apocenter goes to infinity, the pericenter coincide with the turning point of the trapped orbits to be the unstable MCO, and the root structure composed with whirling trapped orbits and whirling deflecting orbits read as  $|+\bullet\bullet+$ . While for other points on this curve, the double root separate into the pericenter and the turning point, form the root structure composed with trapped orbits and marginal deflecting orbits as  $|+\bullet-\bullet+$ . Note that when  $e > 1$ , the apocenter becomes negative, the critical parameter value still expressed as (5), and shows similar behavior as that in Figure 5, which is over the line  $e = 1$ . The polar points of the curves with  $e > 1$  denoting the critical value for the disappearance of unstable circular motion with  $E > 1$ , so does the related whirling trapped and whirling deflecting orbits in the root structure  $|+\bullet\bullet+$ . And the other points on the curve denoting the critical values of the disappearance of deflecting orbits in  $|+\bullet-\bullet+$ .

In classical gravity, the aspects on the geodesic motion has been widely studied. Normally in classical gravity, the bound orbital motion has non-zero angular momentum, such that the ingoing and out going particle motion divided by the turning points are not along the same path, and instead move around the black hole for several circles described by the well known

rational numbers [30]. The whirling deflecting orbits with  $E \geq 1$  in the  $+$  region of  $\bullet\bullet + \rangle$  describes the free falling motion start from far infinity with proper selected energy and angular momentum in the phase space, and in the end asymptotically close to the unstable circular orbits around the black hole. Similarly for homoclinic orbits in the  $+$  region of  $\bullet\bullet + \bullet - \rangle$  with  $E < 1$ , except the motion is not start from the infinity, but from some point between the turning point and the unstable circular motion. The deflecting orbital motion in the  $+$  region of  $- \bullet + \rangle$  with  $E > 1$ , also starts from far infinity, and in the end moves to infinity, during the period of which, it may move around the black hole for several circles to reach the turning point, and then other several circles to fly away the black hole. All these generic motion classes normally moves around the black hole with several circles, even though not as a whole circle sometimes, at least produce the non-zero azimuthal change  $\Delta\phi$ , such that when touching the turning point, the motion is not directly bounce back to the original coming path, and instead chose another direction to leave.

However, in effective quantum gravity, the geodesic motion are interestingly different, especially the motion with the critical value. On the curves with exactly the critical value  $\alpha = \alpha_{bc}$ , the orbits still exists with zero angular momentum  $L = 0$ , which implicates an interesting phenomena that the effective quantum gravity does not only attract, but also repulse. In Section 3, we discussed that at the critical point, the particle will be static lavitating at the position, where the disappeared circular motion should be. This preliminary shows the repulsive effect of the quantum gravity. Moreover, in the bound and deflecting cases, the repulsive effect is even more obvious.

For the bound orbits with critical value  $\alpha = \alpha_{bc}$ , we can set a free falling particle, with initial energy and angular momentum proper selected in the phase space, at any point  $r_b$  between  $r_p$  and  $r_a$ , such that  $r_p < r_b < r_a$ . The radial potential at the turning points are zero  $R(r_a) = R(r_p) = 0$ , and between  $r_p$  and  $r_a$  are positive, such that there exists a polar point we defined as  $r_o$  that satisfies  $R'(r) = 0$  and  $r_p < r_o < r_a$ . Then the particle falls straight to the pericenter, and then directly turns back to the apocenter along the same ingoing path, since the angular momentum of the motion is zero. Therefore the whole bound motion behaves exactly as same as the kinetic spring motion, bouncing directly between  $r_a$  and  $r_p$ , without passing circles around the black hole. For the ingoing motion, the gravity shows attractive effect when the particle moves in the region  $r_o < r < r_a$ , and repulsive effect in the region  $r_p < r < r_o$ .

For the critical homoclinic orbits with  $E < 1$ , which moves between the apocenter  $r_a$  and the double root  $r_*$ , the free falling particle straightly moves forward to  $r_*$ , and stops at the critical unstable circular position  $r_*$  and then hang over there in the end. Similarly for the critical whirling deflecting orbits with  $E \geq 1$ , the particle falls from far infinity, and hangs at the critical unstable circular position in the end.

For the critical deflecting orbits with  $E \geq 1$ , the particle could fall freely from far infinity, and moves straightly to the turning points, then directly bounce back to infinity along exactly the ingoing path. Such kind of geodesic motion clearly shows the repulsive effect in the covariant effective loop quantum gravity. Note that there still exists a polar point  $r_p < r_o < \infty$  for the

critical deflecting orbits, such that when the particle freely moves in the region  $r_o < r < \infty$ , the gravity shows attractive effect, and in the region  $r_p < r < r_o$ , the gravity shows repulsive effect.

## 5 Conclusion and discussion

In this work, we discussed the behavior of the geodesic motion around the black hole model in effective quantum gravity. We found that there exists critical values of the quantum correction parameter, beyond which all classes of geodesic motion in  $(E, L)$  phase space starts to disappear, including ISCO, generic circular motion, periodical bound motion, deflecting motion, and the motion related to them.

We analytically discussed the critical behavior of various types of geodesic motion and provided an explicit determination of the corresponding critical parameters. Our results revealed that the critical circular geodesic motion deviated from the conventional sense of circular motion, instead resembling a static point suspended in space. This finding suggested the existence of static, free test particles around the quantum black holes within the framework of covariant effective quantum gravity.

We compared the behavior of geodesic motion with turning points in classical gravity and covariant effective quantum gravity. Due to the vanishing angular momentum, the critical periodic bound orbital motion transitioned into the oscillatory motion between the pericenter and apocenter. And, the critical homoclinic and whirling deflecting orbital motions asymptotically settled at their respective circular positions in their own root structures. Most notably, the behavior of critical deflecting orbits provided clear evidence that the covariant loop effective quantum gravity introduced a repulsive component to the gravitational interaction, supplementing the familiar attractive force.

The emergence of the repulsive gravitational regime in covariant EQG carries significant implications for our understanding of gravity near the Planck scale. Traditionally, gravitational attraction is taken as a universal property, with orbits and trajectories around black holes governed by purely attractive potentials. The appearance of static free test particles and repulsive like behavior challenges this classical intuition and suggests that quantum effects could drastically modify gravitational dynamics. Especially when the quantum parameter dominates, the size of the quantum black hole is in Planck scale, where the quantum effect dominates, which may cause this anti-intuitive behavior.

## Acknowledgments

We would like to thank Cong Zhang, Wencong Gan, and Chen Lan for helpful discussions. Y. L. is financially supported by Natural Science Foundation of Shandong Province under Grants No.ZR2023QA133 and Yantai University under Grants No.WL22B218. Jie Jiang is

supported by the National Natural Science Foundation of China with Grant No.12205014, the Guangdong Basic and Applied Research Foundation with Grant No.2021A1515110913. Bing Sun is supported by the National Natural Science Foundation of China under Grants No.12375046 and No.12475046 and Beijing University of Agriculture under Grants No.QJKC-2023032.

## References

- [1] F. Hofmann and J. Müller, “Relativistic tests with lunar laser ranging,” *Class. Quant. Grav.* **35** (2018), no. 3, 035015.
- [2] A. Genova, E. Mazarico, and J. Goossens et al. , “Solar system expansion and strong equivalence principle as seen by the NASA MESSENGER mission.,” *Nat Commun* **9** (2018), no. 289,.
- [3] **LIGO Scientific, Virgo** Collaboration, B. P. Abbott *et al.*, “Observation of Gravitational Waves from a Binary Black Hole Merger,” *Phys. Rev. Lett.* **116** (2016), no. 6, 061102, 1602.03837.
- [4] **ET** Collaboration, M. Maggiore *et al.*, “Science Case for the Einstein Telescope,” *JCAP* **03** (2020) 050, 1912.02622.
- [5] C. Rovelli and L. Smolin, “Knot Theory and Quantum Gravity,” *Phys. Rev. Lett.* **61** (1988) 1155.
- [6] J. Ambjorn, J. Jurkiewicz, and R. Loll, “Dynamically triangulating Lorentzian quantum gravity,” *Nucl. Phys. B* **610** (2001) 347–382, hep-th/0105267.
- [7] T. Clifton, P. G. Ferreira, A. Padilla, and C. Skordis, “Modified Gravity and Cosmology,” *Phys. Rept.* **513** (2012) 1–189, 1106.2476.
- [8] S. Surya, “The causal set approach to quantum gravity,” *Living Rev. Rel.* **22** (2019), no. 1, 5, 1903.11544.
- [9] T. Thiemann, *Modern Canonical Quantum General Relativity*. Cambridge Monographs on Mathematical Physics. Cambridge University Press, 2007.
- [10] J. F. Donoghue, “The effective field theory treatment of quantum gravity,” *AIP Conf. Proc.* **1483** (2012), no. 1, 73–94, 1209.3511.
- [11] R. Jha, “Introduction to Hamiltonian formulation of general relativity and homogeneous cosmologies,” *SciPost Phys. Lect. Notes* **73** (2023) 1, 2204.03537.

- [12] M. Bojowald and G. M. Paily, “Deformed General Relativity and Effective Actions from Loop Quantum Gravity,” *Phys. Rev. D* **86** (2012) 104018, 1112.1899.
- [13] C. Zhang, J. Lewandowski, Y. Ma, and J. Yang, “Black Holes and Covariance in Effective Quantum Gravity,” 2407.10168.
- [14] G. Compère, K. Fransen, T. Hertog, and J. Long, “Gravitational waves from plunges into Gargantua,” *Class. Quant. Grav.* **35** (2018), no. 10, 104002, 1712.07130.
- [15] M. van de Meent, “Gravitational self-force on generic bound geodesics in Kerr spacetime,” *Phys. Rev. D* **97** (2018), no. 10, 104033, 1711.09607.
- [16] E. Poisson, A. Pound, and I. Vega, “The Motion of point particles in curved spacetime,” *Living Rev. Rel.* **14** (2011) 7, 1102.0529.
- [17] V. Perlick and O. Y. Tsupko, “Calculating black hole shadows: Review of analytical studies,” *Phys. Rept.* **947** (2022) 1–39, 2105.07101.
- [18] Y. Hou, Z. Zhang, H. Yan, M. Guo, and B. Chen, “Image of a Kerr-Melvin black hole with a thin accretion disk,” *Phys. Rev. D* **106** (2022), no. 6, 064058, 2206.13744.
- [19] R. Penrose and R. M. Floyd, “Extraction of rotational energy from a black hole,” *Nature* **229** (1971) 177–179.
- [20] D. N. Page and K. S. Thorne, “Disk-Accretion onto a Black Hole. Time-Averaged Structure of Accretion Disk,” *Astrophys. J.* **191** (1974) 499–506.
- [21] L. Sadeghian, F. Ferrer, and C. M. Will, “Dark matter distributions around massive black holes: A general relativistic analysis,” *Phys. Rev. D* **88** (2013), no. 6, 063522, 1305.2619.
- [22] Y. Liu and B. Sun, “Analytical solutions of equatorial geodesic motion in Kerr spacetime\*,” *Chin. Phys. C* **48** (2024), no. 4, 045107, 2305.11045.
- [23] G. Compère, Y. Liu, and J. Long, “Classification of radial Kerr geodesic motion,” *Phys. Rev. D* **105** (2022), no. 2, 024075, 2106.03141.
- [24] A. Druart, *The Motion of Test Bodies around Kerr Black Holes*. PhD thesis, U. Brussels, 2023. 2307.02589.
- [25] Z. Cai, M. Liu, T.-Y. He, W.-Q. Wang, Z.-W. Han, and R.-J. Yang, “Analysis of the Geodesic Motions of Massive Particles in Kerr–Sen–AdS<sub>4</sub> Spacetime,” *Universe* **10** (2024), no. 3, 133, 2305.12466.
- [26] A. Cieřlik, E. Hackmann, and P. Mach, “Kerr geodesics in terms of Weierstrass elliptic functions,” *Phys. Rev. D* **108** (2023), no. 2, 024056, 2305.07771.

- [27] N. Sanchis-Gual, C. Herdeiro, E. Radu, J. C. Degollado, and J. A. Font, “Numerical evolutions of spherical Proca stars,” *Phys. Rev. D* **95** (2017), no. 10, 104028, 1702.04532.
- [28] K. Glampedakis and D. Kennefick, “Zoom and whirl: Eccentric equatorial orbits around spinning black holes and their evolution under gravitational radiation reaction,” *Phys. Rev. D* **66** (2002) 044002, gr-qc/0203086.
- [29] Y. Du, Y. Liu, and X. Zhang, “Spinning Particle Dynamics and ISCO in Covariant Loop Quantum Gravity,” 2411.13316.
- [30] J. Levin and G. Perez-Giz, “A Periodic Table for Black Hole Orbits,” *Phys. Rev. D* **77** (2008) 103005, 0802.0459.